Available online at https://link.springer.com/journal/42241
http://www.jhydrodynamics.com
Journal of Hydrodynamics, 2020, 32(2): 286-295
https://doi.org/10.1007/s42241-020-0022-4

Vortex identification methods in marine hydrodynamics *

Wei-wen Zhao, Jian-hua Wang, De-cheng Wan
Computational Marine Hydrodynamics Lab (CMHL), School of Naval Architecture, Ocean and Civil Engineering, State Key Laboratory of Ocean Engineering, Shanghai Jiao Tong University, Shanghai 200240, China

(Received January 9, 2020, Revised January 16, 2020, Accepted January 17, 2020, Published online April 23, 2020)

Abstract: In this paper, several commonly used vortex identification methods for marine hydrodynamics are revisited. In order to extract and analyse the vortical structures in marine hydrodynamics, the Q, λ_2-criterion and modified normalized Liutex/Rortex $\tilde{\Omega}_R$ method are utilized for vortex identification for propeller open water test, ship drag test, ship propeller-rudder interaction, VIV of a marine riser and VIM of a Spar platform. The limitation of Q and λ_2-criterion is discussed. The Liutex/Rortex $\tilde{\Omega}_R$ method is promising for convenient and accurate vortex identification and visualization. However, care should be taken when choosing the small parameter b_0 for $\tilde{\Omega}_R$. We proposed recommended values of b_0 for marine hydrodynamic problems.

Key words: Marine hydrodynamics, vortex identification, Omega, Liutex/Rortex, naoe-FOAM-SJTU solver, OpenFOAM

Introduction

Marine hydrodynamic flows are turbulent and disordered, not only because the flow is usually at high Reynolds number, but also due to the complexity of wall-bounded flow especially for those involving complex geometries. These two main factors lead to the ubiquitous vortex structures. For example, the tip and hub vortex of a rotating propeller[1-2], the vortices shed from ship hull when performing large drift angle maneuvering[3-4], the vortices shed from appendages (such as bilge, fin) of a fully appended ship[5-6], vortex shedding of deep-draft column stabilized floaters[7-9], etc.. In the past, the research of marine hydrodynamics was focused on macroscopic quantities such as forces, moments and motions due to the limitation of experimental facilities and potential theory methods. However, the advancement of particle imagine velocimetry (PIV) and computational fluid dynamic (CFD) for viscous flow makes it possible to provide detailed flow field information. Researchers are paying more and more attentions on the analysis of vortex structures for hydrodynamics. By extracting and studying the vortex dynamics, researchers can have a deep insight of the detailed flow field such as pressure fluctuation, loads, vibrations and fatigue on structures.

Typically, vortex can be visualized by regions or lines[10]. The region method takes vortex as a connected region and uses isosurfaces to identify vortex. The isosurfaces could describe the extended distance from the vortex core. The line method tracks the trajectory of fluid particle through extracting the cores of swirl motion in given area[11]. These two class of visualization methods are complementary to each other for different purposes. Vortex identification methods can be categorized into either Eulerian or Lagrangian. The first type uses Eulerian quantities such as velocity, pressure to help identifying vortex. The second type is usually based on the trajectory of fluid particle motions.

In the current study, we first review several Eulerian vortex identification methods in detail and discuss the relative merits of these methods. Then selective numerical examples of marine hydrodynamic problems are processed by the Q, λ_2-criterion and modified normalized Liutex/Rortex $\tilde{\Omega}_R$ method. The

* Project supported by the National Natural Science Foundation of China (Grant Nos. 51909160, 51879159), the National Key Research and Development Program of China (Grant Nos. 2019YFB1704200, 2019YFC0312400).
Biography: Wei-wen Zhao (1990-), Male, Ph. D., Assistant Professor, E-mail: weiwen.zhao@sjtu.edu.cn
Corresponding author: De-cheng Wan, E-mail: dcwan@sjtu.edu.cn

strengths and weaknesses of different methods are discussed based on the extracted and visualized vortex structures.

1. Vortex identification methods

To study the behaviour of vortices, the vortex structures should first be identified and extracted from the flow field. This section outlines the most commonly used vortex identification methods in marine hydrodynamics.

1.1 *Vorticity*

Vorticity is defined as the curl of velocity. It can be written in the following formula

$$\boldsymbol{\omega} \equiv \nabla \times \boldsymbol{u} \tag{1}$$

It is undoubtfully that the magnitude of vorticity is the most widely used quantity to represent vortex cores for free shear flows, especially for 2-D case. However, vorticity magnitude is not necessarily an appropriate vortex identifier for wall-bounded flows because vorticity includes both the near-wall shear motion and swirling motion. The swirling part cannot be extracted from vorticity. For example, in 2-D wall-bounded flow, the maxima and minima of vorticity magnitude occur at the wall, where a vortex obviously does not exist. The large-scale vorticity is due to the strong shear effect of boundary layer in near wall region. In addition, vorticity cannot identify vortex cores in shear flows if the background shear is comparable to the vorticity magnitude[12]. Vorticity is a necessary, but not a sufficient condition for vortical motion. Thus vorticity is not suitable nor accurate to identify vortex.

1.2 *Methods based on velocity gradient*

Due to the shortcoming of vorticity for identifying vortex, several methods based on the local characteristics of velocity gradient are proposed. As the velocity gradient tensor is independent of different Galilean frames of reference, these methods are Galilean invariant.

The characteristic polynomial equation of velocity gradient tensor $\nabla \boldsymbol{u}$ can be given by the following formula

$$\lambda^3 - P\lambda^2 + Q\lambda - R = 0 \tag{2}$$

where λ is the eigenvalue of $\nabla \boldsymbol{u}$, P, Q and R are the first, second and third invariant of $\nabla \boldsymbol{u}$, respectively. They are defined as

$$P = \mathrm{tr}(\nabla \boldsymbol{u}) \tag{3}$$

$$Q = \frac{1}{2}\{[\mathrm{tr}(\nabla \boldsymbol{u})]^2 - \mathrm{tr}[(\nabla \boldsymbol{u})^2]\} \tag{4}$$

$$R = \det(\nabla \boldsymbol{u}) \tag{5}$$

in which, tr and det represent the trace and determinant of the 3×3 tensor, respectively.

By decomposition, the velocity gradient tensor is split into two parts, written by

$$\nabla \boldsymbol{u} = \boldsymbol{S} + \boldsymbol{\Omega} \tag{6}$$

where $\boldsymbol{S}$ is a symmetric tensor called strain rate tensor, and $\boldsymbol{\Omega}$ is a skew symmetric tensor called spin tensor or rotation rate tensor.

1.2.1 Q-criterion

The Q-criterion is one of the most commonly used vortex identification methods[2-3]. It borrows the definition directly from the second invariant of velocity gradient tensor. For incompressible flow, the trace of $\nabla \boldsymbol{u}$ is 0. Thus Q can be simplified as

$$Q = \frac{1}{2}(\|\boldsymbol{\Omega}\|^2 - \|\boldsymbol{S}\|^2) \tag{7}$$

where the $\| \ \|$ notation stands for Frobenius norm of a tensor. $\|\boldsymbol{\Omega}\|$ and $\|\boldsymbol{S}\|$ are defined by

$$\|\boldsymbol{\Omega}\| = \sqrt{\mathrm{tr}(\boldsymbol{\Omega}^{\mathrm{T}}\boldsymbol{\Omega})} \tag{8}$$

$$\|\boldsymbol{S}\| = \sqrt{\mathrm{tr}(\boldsymbol{S}^{\mathrm{T}}\boldsymbol{S})} \tag{9}$$

Q-criterion defines a vortex as a "connected fluid region with a positive second invariant of $\nabla \boldsymbol{u}$"[13], which essentially means the rotational force is larger than the shear force.

1.2.2 λ_2-criterion

The λ_2-criterion method is also widely used in marine hydrodynamic flows[14]. It looks for the pressure minimum region by performing gradient calculation of Naviers-Stokes equation and decomposes it into symmetric and antisymmetric parts[12]. The contribution of unsteady straining and viscous effects is discarded and only $\boldsymbol{S}^2 + \boldsymbol{\Omega}^2$ is considered. By calculating and sorting the eigenvalues of $\boldsymbol{S}^2 + \boldsymbol{\Omega}^2$ in descending order (e.g., $\lambda_1 > \lambda_2 > \lambda_3$) and taking the second eigenvalue λ_2 as the criterion to identify vortex, λ_2-criterion defines "a vortex core as a connected region with two negative eigenvalues of $\boldsymbol{S}^2+\boldsymbol{\Omega}^2$ ", which equivalently means $\lambda_2<0$. However, in situations where several vortices exists, it can be difficult for this method to distinguish between individual vortices.

1.2.3 Ω method

According to Liu et al.[15], the vorticity of fluid can be divided into vortical and non-vortical parts. This is crucial to identify and extract pure rotational motions from fluids. Boundary layer transition of a flat plane, for instance, contains large vorticity regions near boundaries. But the flow is parallel and there are no rotational motions. Based on this point of view, the Ω method defines a normalized scalar represents the ratio of rotational and shear motion, given by

$$\Omega=\frac{\|\boldsymbol{\Omega}\|^2}{\|\boldsymbol{S}\|^2+\|\boldsymbol{\Omega}\|^2+\varepsilon} \tag{10}$$

where ε is a small positive number used to avoid division by zero and is given by $\varepsilon=10^{-3}\max(\|\boldsymbol{\Omega}\|^2-\|\boldsymbol{S}\|^2)$.

The normalized Ω has a clear physical meaning. When the rotation strength is larger than deformation (i.e., $\Omega>0.5$), vortex exists in this region. In practice, $\Omega=0.52$ is recommended. This method can capture both the strong and weak vortices due to the definition is a relative ratio rather than an absolute value.

1.2.4 Liutex/Rortex method

As the skew symmetric tensor $\boldsymbol{\Omega}$ cannot represent the rigid rotational motion, the Liutex/Rortex method[16-20] is proposed to address the issues of how to extract rigid rotational part from the fluid motion. The strict definition of Liutex vector can be summarized as follows:

(1) The direction of Liutex vector $\boldsymbol{r}$

If the velocity gradient tensor $\nabla\boldsymbol{u}$ has three real eigenvalues, that means the fluid motion only contains stretch and deforming. In such condition, the magnitude of Liutex vector is zero. On the contrary, if $\nabla\boldsymbol{u}$ has one real and two conjugate complex eigenvalues, there exists vortex in this local region. The Liutex vector is aligned with the direction of eigenvector corresponding to the only real eigenvalue. The normalized eigenvector is marked as $\boldsymbol{r}$.

(2) The magnitude of Liutex vector R

By transforming the original coordinate system xyz to a new coordinate system XYZ with a transform matrix $\boldsymbol{Q}$, the original z-axis is rotated to the direction of $\boldsymbol{r}$. In the new coordinate system, fluid will only rotate in the XY plane, i.e., the Z-direction derivatives of U_X and U_Y are zero. After rotation, the velocity gradient tensor becomes

$$\nabla\boldsymbol{U}=\boldsymbol{Q}\nabla\boldsymbol{u}\boldsymbol{Q}^{\mathrm{T}}=\begin{bmatrix}\frac{\partial U_X}{\partial X} & \frac{\partial U_X}{\partial Y} & 0\\ \frac{\partial U_Y}{\partial X} & \frac{\partial U_Y}{\partial Y} & 0\\ \frac{\partial U_Z}{\partial X} & \frac{\partial U_Z}{\partial Y} & \frac{\partial U_Z}{\partial Z}\end{bmatrix} \tag{11}$$

$\boldsymbol{Q}$ is the transform matrix which can be obtained by the formula given in references[16, 18].

By a second transformation with matrix $\boldsymbol{P}$ which rotates the Z-axis by θ, the velocity gradient tensor becomes

$$\nabla\boldsymbol{U}_P=\boldsymbol{P}\nabla\boldsymbol{U}\boldsymbol{P}^{\mathrm{T}} \tag{12}$$

with $\boldsymbol{P}$ defined by

$$\boldsymbol{P}=\begin{bmatrix}\cos\theta & \sin\theta & 0\\ -\sin\theta & \cos\theta & 0\\ 0 & 0 & 1\end{bmatrix} \tag{13}$$

The rotating angle θ is calculated to ensure the absolute value of $\partial U_X/\partial Y|_\theta$ is minimum. The magnitude of Liutex vector is then given by

$$R=2(\beta-\alpha),\quad \beta^2>\alpha^2 \tag{14a}$$

$$R=0,\quad \alpha^2\geq\beta \tag{14b}$$

in which

$$\alpha=\frac{1}{2}\sqrt{\left(\frac{\partial U_Y}{\partial Y}-\frac{\partial U_X}{\partial X}\right)^2+\left(\frac{\partial U_Y}{\partial X}+\frac{\partial U_X}{\partial Y}\right)^2} \tag{15}$$

$$\beta=\frac{1}{2}\left(\frac{\partial U_Y}{\partial X}-\frac{\partial U_X}{\partial Y}\right) \tag{16}$$

(3) The Liutex vector is obtained by $\boldsymbol{R}=R\boldsymbol{r}$

To simplify computational procedure of Liutex vector, Wang et al.[21] gave an explicit formula of Liutex vector

$$\boldsymbol{R}=\left(\langle\boldsymbol{\omega},\boldsymbol{r}\rangle-\sqrt{\langle\boldsymbol{\omega},\boldsymbol{r}\rangle^2-4\lambda_{ci}^2}\right)\boldsymbol{r} \tag{17}$$

where λ_{ci} is the imaginary part of eigenvectors corresponding to the conjugate complex eigenvalues of $\nabla \boldsymbol{u}$.

The author claims that by using the explicit formula, the calculation efficiency for Liutex can be dramatically improved by 37%[21], which is rather impressive. From the formula, it is easy to judge that Liutex vector involves the eigenvalues, eigenvectors of velocity gradient tensor, as well as local vorticity. Furthermore, Liutex vector implies not only the rotation strength but also the rotation axis of the local fluid motion. The physical meaning is rather clear, it decomposes vorticity into the vortical part $\boldsymbol{R}$ and non-vortical part $\boldsymbol{\omega}-\boldsymbol{R}$ and only uses the vortical part to represent vortex.

1.2.5 Ω - Liutex method

By combining the advantages of Ω and Liutex methods, Dong et al.[19] proposed the normalized Liutex method which defines a scalar Ω_R with the following formula

$$\Omega_R = \frac{\beta^2}{\alpha^2 + \beta^2 + \varepsilon} \tag{18}$$

The formula is very similar to the Ω method. The parameters α and β are borrowed from Liutex vector and their definitions can be found in Eqs. (15) and (16). $\varepsilon = b_0 \max(\beta^2 - \alpha^2)$ is a small parameter to avoid division by zero and b_0 is a small positive number around 0.001-0.002.

The combined method shows promising results. It can not only measure the relative rotation strength on the plane perpendicular to the local rotation axis, but also separate rotational vortices from shear layers, discontinuity structures and other non-physical structures. However, Liu and Liu[20] found that the extracted isosurfaces formed by Ω_R is not smooth enough and contain many bulges. They improved it and proposed the modified normalized $\tilde{\Omega}_R$ method, whose formula is given by

$$\tilde{\Omega}_R = \frac{\beta^2}{\alpha^2 + \beta^2 + \lambda_{cr}^2 + 0.5\lambda_r^2 + \varepsilon} \tag{19}$$

where λ_{cr} and λ_r are real part of conjugate complex eigenvalues and real eigenvalues of velocity gradient tensor, respectively.

With the help of explicit Liutex formula, the above equation can be rewritten as follows

$$\tilde{\Omega}_R = \frac{(\boldsymbol{\omega}\cdot\boldsymbol{r})^2}{2[(\boldsymbol{\omega}\cdot\boldsymbol{r})^2 - 2\lambda_{ci}^2 + 2\lambda_{cr}^2 + \lambda_r^2] + \varepsilon} \tag{20}$$

1.3 *Other methods*

1.3.1 Helicity

The helicity is introduced by Levy et al.[22] to extract vortex core lines. The normalized helicity is given by a scalar quantity defined by

$$H_n = \frac{\boldsymbol{\omega}\cdot\boldsymbol{u}}{|\boldsymbol{\omega}||\boldsymbol{u}|} \tag{21}$$

From the above formula, it is clear and obvious that H_n represents the cosine of the angle between velocity and vorticity. It assumes that in the near vortex core regions, velocity and vorticity have small angles such that H_n gives the maximum value. The vortex core can be identified by locating the maxima of H_n. Moreover, helicity can represent the strength of primary and secondary vortex. When the sign of helicity switches, it indicates the transition between primary and secondary vortex. Thus the helicity scalar is usually used for dyeing colour of vortical structures.

1.3.2 Pressure method

For 2-D flow, pressure minimum always occurs at the rotation centre of the fluid. It is therefore reasonable to extract rotation of fluid by locating the minima of pressure. By tracing the sectionally local minimum of pressure, the disconnected vortex filament can be extracted[23]. However, this method is not suitable for unsteady, viscous and 3-D flow.

2. Numerical approaches

In this section, we choose several typical flows in marine hydrodynamics to demonstrate the characteristics of several vortex identification methods. All the selected examples are numerically computed using the naoe-FOAM-SJTU solver[24-26], which is developed on top of the OpenFOAM framework. It utilizes the data structures and low-level infrastructures of OpenFOAM and consists of several specialized features for marine hydrodynamics. Figure 1 shows the functional modules of the solver, in which the blue where the blue frame and red frame represent developed and developing modules, respectively.

The calculation of Q and λ_2 are provided in OpenFOAM's *function object* framework as postprocessing utilities. Similarly, we implemented Ω, Liutex and Ω - Liutex methods under the frame work of *function object* as postprocessing utilities. In such a way these vortex identification methods can be applied to arbitrary unstructured polyhedral computational mesh with complex geometries.

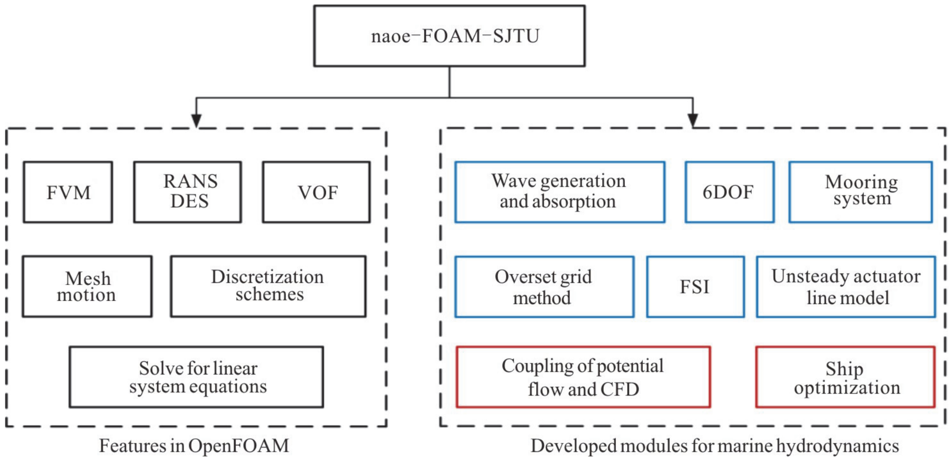

Fig. 1 (Color online) Main framework of naoe-FOAM-SJTU solver[27]

The comparisons between Ω, Liutex and Ω-Liutex have been discussed extensively. In this paper, we compare Q and λ_2 methods with the most recently proposed $\tilde{\Omega}_R$ method. Recalling that the small parameter b_0 in $\tilde{\Omega}_R$ method is defined to prohibit the computational noise and avoid dividing by zero[20]. The default value of b_0 is recommended to set as a value between 0.001 and 0.002. However, this value is not suitable for typical marine hydrodynamic flows. We will discuss the applicable values of b_0 for marine hydrodynamic flows in Section 4.

3. Applications of vortex identification methods

3.1 *Propeller open water*

In this subsection, a propeller open water test case is used for demonstration. The model is a four-bladed propeller for the ONR Tumblehome (ONRT) model 5613 which is a modern surface combatant and publicly available for fundamental research[28]. Some studies of the hydrodynamic performance of the propeller have been published in previous work[29]. The propeller is simulated using dynamic overset grid and the open water curves are obtained by a single-run procedure. Two mesh blocks were generated for background and propeller individually and assembled to a single overset grid system. Here we show the condition of advance coefficient $J = V_A/(nD_P) = 0.9$, where V_A is the advance speed, n and D_P are the rotational speed and diameter of propeller, respectively.

Figure 2 shows isosurfaces of different λ_2 values coloured with vorticity magnitude. The tip vortices of the propeller are resolved clearly. However,

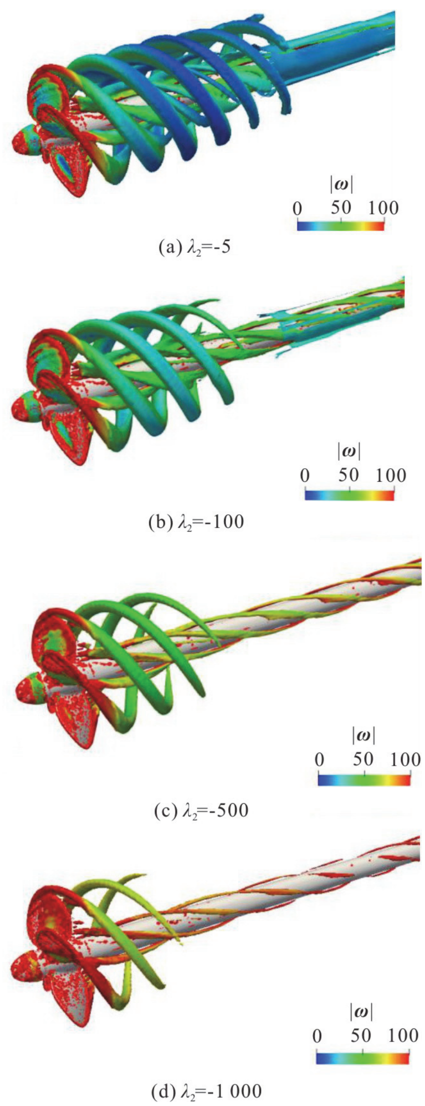

Fig. 2 (Color online) Propeller operating at $J = 0.9$. Isosurfaces of different λ_2-criterion, coloured by vorticity magnitude

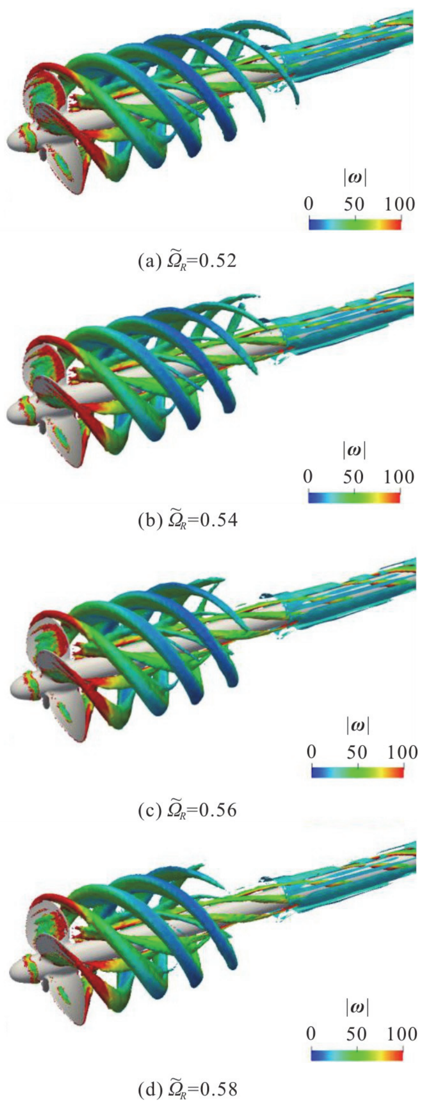

Fig. 3 (Color online) Propeller operating at $J = 0.9$. Isosurfaces of different $\tilde{\Omega}_R$, coloured by vorticity magnitude

using different Q values as the threshold for contour, various length of tip vortices are extracted. For small λ_2 values shown in Fig. 2(a), more detailed wake structures are identified and extracted. As threshold of Q increases, those weak vortex (fluid regions with smaller vorticity magnitude) cannot be identified. The structures of vortex filament are also distinct. The vortex tube extracted by larger Q threshold value is thinner. Figure 3 shows the propeller wake structures which are identified and extracted by different values of modified normalized Rortex $\tilde{\Omega}_R$ and coloured by vorticity magnitude. The contour threshold value 0.52 is the recommended value in the original paper[20]. Besides this, we also choose three other threshold values for comparison. As depicted in the pictures, although the vortex lengths in wake region are different, the vortex tube structures extracted by different $\tilde{\Omega}_R$ values and the corresponding vorticities remain keep almost the same.

3.2 *Ship drag test*

Japan Bulk Carrier (JBC) is another model of benchmark case for the Tokyo 2015 CFD workshop. It is a full form ship with a block coefficient up to 0.858. The bare hull is drag in still water with a towing speed of 1.179 m/s, corresponding to $Fr = 0.142$ and $Re = 7.46 \times 10^7$. In this study, the turbulence is modelled by delayed detached-eddy simulations (DDES) and the total grid number is 7.48×10^6. Details about the computational setup can be referred to Wang and Wan[30].

Figures 4 and 5 illustrate the vortical structures extracted by Q-criterion and modified normalized Rortex method, respectively. The vortex above free surfaces are eliminated for sake of simplicity. At first glance, the two figures shows similar vortex structures. In the vicinity of stern, massively separation flow due to the sharp curvature change of the hull surface is observed. The captured structures is, however, very distinctive. In Fig. 4, the vortices identified by Q contain redundant shear motions near the hull surface. These deformations is excluded in the vortices extracted by $\tilde{\Omega}_R$.

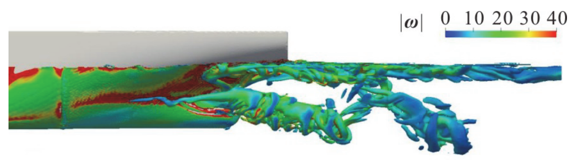

Fig. 4 (Color online) Vortical structures in wake region presented by isosurfaces with $Q = 5$ and coloured by vorticity magnitude

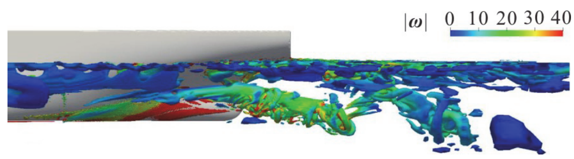

Fig. 5 (Color online) Vortical structures in wake region presented by isosurfaces with $\tilde{\Omega}_R = 0.52$ and coloured by vorticity magnitude

3.3 *Ship propeller-rudder interaction*

The propeller-rudder interaction of the ONRT surface combatant during a zigzag maneuver is visualized. Detailed results of the maneuvering study will be published on the SIMMAN2020 workshop. The simulation follows the SIMMAN2020 case 5.2.2, corresponding to a 20/20 zigzag test, starting to starboard side. The model is scaled at a ratio of 1:48.935 and is self-propelled with free running, which means all six degrees of freedoms for the model are released, at model point in calm water. The corresponding Froude and Reynolds number are $Fr = 0.200$ and $Re = 3.39\times10^6$, respectively. In the 20/20 zigzag maneuver test the rudder is turned to the opposite direction at a rate of 35 °/s to a rudder angle of 20° every time the ship heading reaches ±20°. The computational grid for moving components such as hull, propellers and rudders are generated separately and are then assembled into a composite overset grid. All component grids can translate and rotate freely with respect to other grids.

Figure 6 gives the instantaneous flow visualizations of hull-propeller-rudder interaction for ONRT during zigzag maneuvering. The vortical structures are identified by different criterions and coloured by vorticity magnitude. Similar to the results in Section 3.1, the dominant wake structures are the clockwise and anti-clockwise tip vortices generated by the contra-rotating twin-screw propellers. Strong hub vortices are also observed. Owing to the numerical dissipation and coarse grid resolution in the rudder downstream wake regions, the vorticity of hub vortices become smaller. These weak vortices is not identified by the Q- criterion. However, the $\tilde{\Omega}_R$ method can capture both the weak and strong tip vortices simultaneously

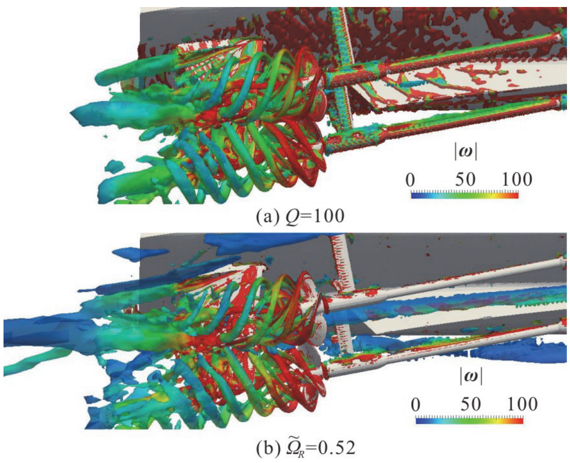

Fig. 6 (Color online) Hull-propeller-rudder interaction of the fully appended ONRT during 20/20 zigzag maneuver test. Isosurfaces by (a), (b) and coloured by vorticity magnitude

Figure 7 depicts another view of the instantaneous vortical structures around the fully appended ONRT model during zigzag maneuver test. Although the simulations are performed using the two-phase VOF model, only vortices in the water are displayed for the sake of simplicity. The rudders have been executed and turned to the port side, which provide lift rudder force. A consequence turning moment turns the ship towards left. The "fake" vortices owing to the boundary layer shear motions near the hull surface such as bow, bilge keel and skeg vortices are removed from the isosurfaces of $\tilde{\Omega}_R = 0.52$. Moreover, isosurfaces of $Q = 100$ can only capture propeller and rudder vortices, with some redundant non-physical vortices near hull, since these are strong vortices and have large vorticity. Other weak vortices generated by free surface ship waves, bilge keel and skeg are failed to be captured by isosurfaces of $Q = 100$, but can be successfully observed in the isosurfaces of $\tilde{\Omega}_R$ = 0.52.

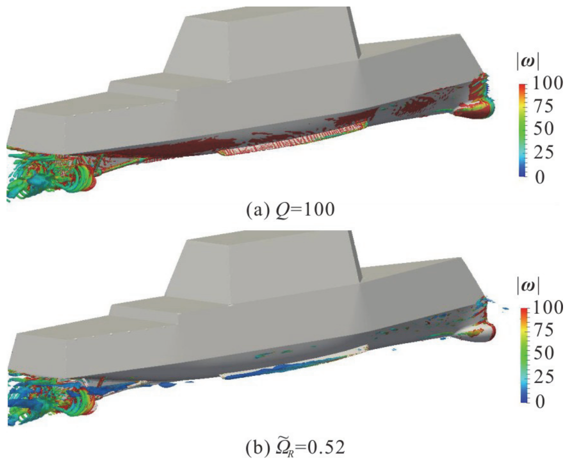

Fig. 7 (Color online) Vortical structures around the fully appended ONRT during 20/20 zigzag maneuver test. Isosurfaces by (a), (b) and coloured by vorticity magnitude

3.4 *VIV of a flexible riser*

Vortex induced vibrations (VIV) is the main cause of marine risers' fatigue damage. It is very hard to predict VIV of marine risers due to the nonlinearity and instability of the flow. By taking the flexible structural deforming into account, the fluid-structure interaction problem become more complex. In this subsection, a riser under stepped flow is simulated. The diameter and length of the riser is 0.028 m and 13.12 m, respectively. Lower part (45% of total length) of the riser is submerged in water with speed of 0.16 m/s. The top is tensioning with a pretension force of 405 N. This case setup is in accordance with the experiment which is performed by Chaplin et al.[31-32]. The VIV of marine riser is simulated by 2.5-D strip method, i.e., the fluid is solved in a finite set of 2-D strip sections and the structure is obtained with 3-D model. In the current solver's implementation, the flow fields in 2-D domains are solved using finite volume method provided by OpenFOAM, and the dynamic structural response is solved using finite element method with Euler-Bernoulli beam model. The hydrodynamic force is obtained from fluid and passed to structure and the displacements are calculated in structure and passed to moving boundaries of fluid mesh in each section.

Figure 8 depicts the 2-D vortices of VIV for a flexible marine riser in fluid sections, represented and coloured by different methods. In both pictures, clear Kármán vortex streets are observed in each section. As been elaborated in previous section, the maxima of vorticity magnitude occurs at the near wall region (Fig. 8(a)). It is convinced that the disadvantages of vorticity magnitude in representing vortices are obvious. Different vortices in the vicinity of wall are identified as a single connected region which is non-physical. Furthermore, the vorticity magnitude is so small in the far wake region that it is hard to distinguish vortical structures. On the other hand, $\tilde{\Omega}_R$, unlike vorticity magnitude, can clearly resolve the individual vortex cores in both near wake region and far wake region.

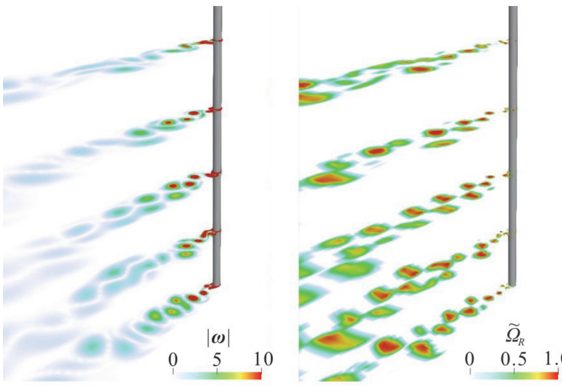

(a) Vorticity magnitude (b) $\tilde{\Omega}_R$

Fig. 8 (Color online) Vortices of VIV for a flexible marine riser in 2-D strip sections.The vortices are represented and coloured by (a), (b)

3.5 *VIM of a spar platform*

Spar platform is a kind of offshore floating product unit with relatively large aspect ratio (draft over diameter). Such kind of floating structures are subject to vortex-induced motions (VIM) when exposed in current with certain speed. The large amplitude oscillating motion is a critical issue for the fatigue failure and safety operations. To mitigate VIM, helical strakes are designed and installed on the surface of main spar hull. A truncated cylindrical hard tank with three-start helical strakes of a truss spar scaled at 1:22.3 is selected for study[33]. Truss structure and keel tank is ignored in the simulation.

Figure 9 shows the instantaneous vortical structures of VIM for the Spar at reduced velocity $U_r = UT_n / D = 6$, with U the current velocity, T_n the natural transverse period and D the diameter of Spar. The vortical structures are represented by the isosurfaces identified with $Q=1$ and $\tilde{\Omega}_R = 0.52$, respectively. The picture vividly illustrates that the dominant vortices shed at the tip of helical strakes. After flow separation, the vortices forms several horseshoe-like vortical structures. This reduces the formation of synchronized shedding of coherent structures along vertical direction and breaks the large-scale eddies into small structures. In such a way, the mitigation of VIM is achieved. Similar to previous results, the $\tilde{\Omega}_R$ method captures strong and weak vortices simultaneously.

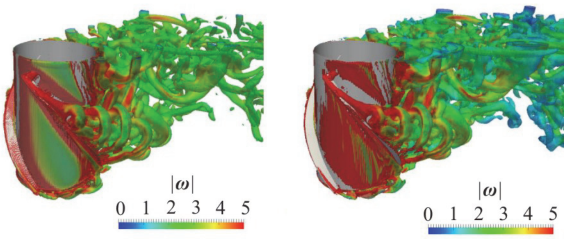

(a) Q=1 (b) $\tilde{\Omega}_R$=0.52

Fig. 9 (Color online) Vortical structures of VIM for a Spar with helical strakes. Isosurfaces by (a), (b) and coloured by vorticity magnitude

4. Discussion on the sensitivity of b_0

According to our numerical tests, we noticed that $b_0 = 0.002$ is too large for typical marine hydrodynamic flows. This is due to the strong fluid rotations can result in large ε which will consequently affect the isosurfaces by $\tilde{\Omega}_R$. If ε is large enough, even if the vortical rotation part strength is larger than non-vortical part, $\tilde{\Omega}_R = 0.52$ will extract wrong vortices which contain non-vortical structures. According to our experience, $b_0 = 10^{-6}$ is suitable for most marine hydrodynamic problems. All the presented results in Section 3 is obtained with this value. However, in some special cases with very strong fluid rotations, $b_0 = 10^{-6}$ is still too large.

We give an example of a self-propelled ONRT in still water to illustrate the sensitivity of b_0 in $\tilde{\Omega}_R$ method. The self-propelled ship is moving forward at model point with moving speed of 1.11 m/s corresponding to Froude number $Fr = 0.200$. The rotational speed is 8.75 RPS obtained with a PI controller which makes sure the propeller thrust is equal to the ship resistance.

Figure 10 shows the vortical structures of the self-propelled ONRT ship at model point. The isosurfaces are extracted by $\tilde{\Omega}_R = 0.52$ with different b_0. For this case, $b_0 = 10^{-3}$ is so large that ε reaches the order of rotation strength magnitude and affects the identification of vortex. No vortices are identified with $b_0 = 10^{-3}$. Even with value $b_0 = 10^{-6}$, the vortices are emerged as thin vortex tube which can be observed in Fig. 10(b). For the zigzag case with same Froude number in Section 3.3, $b_0 = 10^{-6}$ works smoothly. During free running ship zigzag maneuver, the speed loss and oblique inflow make the inflow condition different from self-propulsion. The absolute vortices strength for zigzag maneuver is smaller than self-propulsion condition. Thus large b_0 is reasonable to capture vortices for zigzag maneuver with weaker absolute vortices strength. We suggest b_0 should be set to a small value for flows with strong absolute vortices strength.

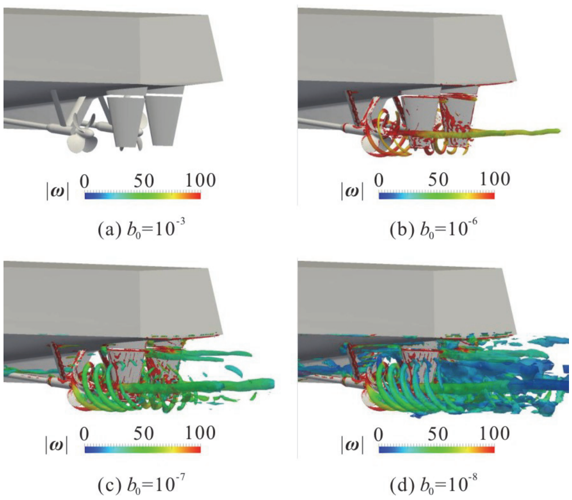

Fig. 10 (Color online) Hull-propeller-rudder interaction of the self-propelled ONRT at model point. Isosurfaces by $\tilde{\Omega}_R = 0.52$

5. Conclusions

In this paper, we first revisit the most commonly used vortex identification methods for marine hydrodynamic flow problems. After that, we introduce the in-house solver naoe-FOAM-SJTU and several numerical examples which are computed by the solver. These classical examples are selected to demonstrate the advantages and disadvantages of different vortex identification methods. After the discussions, the following conclusions can be drawn.

(1) Vortex identification methods such as Q and λ_2-criterion is quite sensitive to the threshold value of isosurface. Hence, it is hard to extract the correct vortical structures for further vortex dynamics analysis.

(2) The Ω-Liutex (modified normalized Rortex) method shows promising results in vortex identification and visualization for marine hydrodynamics. It removes vorticity due to shear motion and only keeps the pure rotational motion part. Furthermore, it can identify strong and weak vortices simultaneously and is insensitive to isosurface threshold value.

(3) For marine hydrodynamic flows which involve strong absolute vortices strength, b_0 should be set to a small value. We recommend that b_0 is set to 10^{-6}.

Acknowledgements

This work was supported by the Chang Jiang Scholars Program (Grant No. T2014099), the Shanghai Excellent Academic Leaders Program (Grant No. 17XD1402300) and the Innovative Special Project of Numerical Tank of Ministry of Industry and Information Technology of China (2016-23/09).

References

[1] Felli M., Falchi M. Propeller wake evolution mechanisms in oblique flow conditions [J]. *Journal of Fluid Mechanics*. 2018, 845: 520-559.

[2] Wang L. Z., Guo C. Y., Su Y. M. et al. A numerical study on the correlation between the evolution of propeller trailing vortex wake and skew of propellers [J]. *International Journal of Naval Architecture and Ocean Engineering*, 2018, 10(2): 212-224.

[3] Xing T., Bhushan S., Stern F. Vortical and turbulent structures for KVLCC2 at drift angle 0, 12, and 30 degrees [J]. *Ocean Engineering*, 2012, 55: 23-43.

[4] Shen Z., Wan D. C., Carrica P. RANS simulations of free maneuvers with moving rudders and propellers using overset grids in OpenFOAM [C]. *SIMMAN Workshop on Verification and Validation of Ship Maneuvering Simulation Methods*, Lyngby, Denmark, 2014.

[5] Sakamoto N., Carrica P. M., Stern F. URANS simulations of static and dynamic maneuvering for surface combatant: Part 2. Analysis and validation for local flow characteristics [J]. *Journal of Marine Science and Technology*, 2012, 17(4): 446-468.

[6] Wang J., Zhao W., Wan D. C. Free maneuvering simulation of ONR tumblehome using overset grid method in naoe-FOAM-SJTU solver [C]. *Proceedings of the 31st Symposium on Naval Hydrodynamics*, Monterey, California, USA, 2016.

[7] Liang Y., Tao L. Interaction of vortex shedding processes on flow over a deep-draft semi-submersible [J]. *Ocean Engineering*, 2017, 141: 427-449.

[8] Liu M., Xiao L., Yang J. et al. Parametric study on the vortex-induced motions of semi-submersibles: Effect of rounded ratios of the column and pontoon [J]. *Physics of Fluids*, 2017, 29(5): 055101.

[9] Zhao W., Zou L., Wan D. et al. Numerical investigation of vortex-induced motions of a paired-column semi-submersible in currents [J]. *Ocean Engineering*, 2018, 164: 272-283.

[10] Epps B. Review of vortex identification methods [C]. *Proceedings of the 55th AIAA Aerospace Sciences Meeting*, Grapevine, Texas, USA, 2017.
[11] Zhang Y., Liu K., Xian H. et al. A review of methods for vortex identification in hydroturbines [J]. *Renewable and Sustainable Energy Reviews*, 2018, 81: 1269-1285.
[12] Jeong J., Hussain F. On the identification of a vortex [J]. *Journal of Fluid Mechanics*, 1995, 285: 69-94.
[13] Haller G. An objective definition of a vortex [J]. *Journal of Fluid Mechanics*, 2005, 525: 1-26.
[14] Fureby C., Anderson B., Clarke D. et al. Experimental and numerical study of a generic conventional submarine at 10° yaw [J]. *Ocean Engineering*, 2016, 116: 1-20.
[15] Liu C., Wang Y., Yang Y. et al. New omega vortex identification method [J]. *Science China Physics, Mechanics and Astronomy*, 2016, 59(8): 684711.
[16] Gao Y., Liu C. Rortex and comparison with eigenvalue-based vortex identification criteria [J]. *Physics of Fluids*, 2018, 30(8): 085107.
[17] Liu C., Gao Y., Tian S. et al. Rortex-A new vortex vector definition and vorticity tensor and vector decompositions [J]. *Physics of Fluids*, 2018, 30(3): 035103.
[18] Liu C., Gao Y. S., Dong X. R. et al. Third generation of vortex identification methods: Omega and Liutex/Rortex based systems [J]. *Journal of Hydrodynamics*, 2019, 31(2): 205-223.
[19] Dong X., Gao Y., Liu C. New normalized Rortex/vortex identification method [J]. *Physics of Fluids*, 2019, 31(1): 011701.
[20] Liu J., Liu C. Modified normalized Rortex/vortex identification method [J]. *Physics of Fluids*, 2019, 31(6): 061704.
[21] Wang Y. Q., Gao Y. S., Liu J. M. et al. Explicit formula for the Liutex vector and physical meaning of vorticity based on the Liutex-Shear decomposition [J]. *Journal of Hydrodynamics*, 2019, 31(3): 464-474.
[22] Levy Y., Degani D., Seginer A. Graphical visualization of vortical flows by means of helicity [J]. *AIAA Journal*, 1990, 28(8): 1347-1352.
[23] Miura H., Kida S. Identification of tubular vortices in turbulence [J]. *Journal of the Physical Society of Japan*, 1997, 66(5): 1331-1334.
[24] Shen Z., Wan D., Carrica P. M. Dynamic overset grids in OpenFOAM with application to KCS self-propulsion and maneuvering [J]. *Ocean Engineering*, 2015, 108: 287-306.
[25] Wang J., Zou L., Wan D. CFD simulations of free running ship under course keeping control [J]. *Ocean Engineering*, 2017, 141: 450-464.
[26] Wang J., Zou L., Wan D. Numerical simulations of zigzag maneuver of free running ship in waves by RANS-Overset grid method [J]. *Ocean Engineering*, 2018, 162: 55-79.
[27] Wang J. H., Zhao W. W., Wan D. C. Development of naoe-FOAM-SJTU solver based on OpenFOAM for marine hydrodynamics [J]. *Journal of Hydrodynamics*, 2019, 31(1): 1-20.
[28] Sanada Y., Tanimoto K., Takagi K. et al. Trajectories for ONR Tumblehome maneuvering in calm water and waves [J]. *Ocean Engineering*, 2013, 72: 45-65.
[29] Wang J., Zhao W., Wan D. Simulations of self-propelled fully appended ship model at different speeds [J]. *International Journal of Computational Methods*, 2019, 16(5): 1840015.
[30] Wang J., Wan D. C. Numerical simulations of viscous flows around jbc ship using different turbulence models [C]. *Proceedings of the 11th International Workshop on Ship and Marine Hydrodynamics*, Hamburg, Germany, 2019.
[31] Chaplin J. R., Bearman P. W., Huera Huarte F. J. et al. Laboratory measurements of vortex-induced vibrations of a vertical tension riser in a stepped current [J]. *Journal of Fluids and Structures*, 2005, 21(1): 3-24.
[32] Chaplin J. R., Bearman P. W., Cheng Y. et al. Blind predictions of laboratory measurements of vortex-induced vibrations of a tension riser [J]. *Journal of Fluids and Structures*, 2005, 21(1): 25-40.
[33] Finnigan T., Roddier D. Spar VIM model tests at supercritical reynolds numbers [C]. *Proceedings of the 26th International Conference on Offshore Mechanics and Arctic Engineering*, San Diego, California, USA, 2007, 3: 731-740.